Observations of the Turkana Jet and the East African Dry Tropics

The RIFTJet Field Campaign

Callum Munday, Sebastian Engelstaedter, Gilbert Ouma, Geoffrey Ogutu, Daniel Olago, Dennis Ong'ech, Thomas Lees, Bonface Wanguba, Rose Nkatha, Clinton Ogalo, Roba Ali Gàlgalo, Abdi Jillo Dokata, Erick Kirui, Robert Hope, and Richard Washington

ABSTRACT: The Turkana low-level jet (LLJ) is an intrinsic part of the African climate system. It is the principle conduit for water vapor transport to the African interior from the Indian Ocean, and droughts in East Africa tend to occur when the jet is strong. The only direct observations of the Turkana jet come from manual tracking of pilot balloons in the 1980s. Now, modern reanalysis datasets disagree with one another over the strength of jet winds and underestimate the strength of the jet by 25%–75% compared to the pilot balloon data. This article gives an overview of a field campaign based in northwest Kenya—the Radiosonde Investigation for the Turkana Jet (RIFTJet)—which measured the Turkana jet for the first time in 40 years using modern technologies. Radiosonde data reveal a persistent low-level jet, which formed on every night of the campaign, with an average low-level maximum wind speed of 16.8 m s^{-1} at 0300 LT. One of the latest reanalysis datasets (ERA5) underestimates low-level wind speeds by an average of 24% (4.1 m s^{-1}) at 0300 LT and by 33% (3.6 m s^{-1}) at 1500 LT. The measurements confirm the role of the Turkana LLJ in water vapor transport: mean water vapor transport at Marsabit is 172 kg m s^{-1}. The dataset provides new opportunities to understand regional dynamics, and to evaluate models in one of the most data-sparse regions in the world.

KEYWORDS: Africa; Atmosphere; Field experiments; Jets; Mesoscale processes; Water vapor

AFFILIATIONS: **Munday, Engelstaedter, Lees, Hope, and Washington**—Climate Research Lab, School of Geography and the Environment, University of Oxford, Oxford, United Kingdom; **Ouma, Olago, Ong'ech, Wanguba, Nkatha, and Ogalo**—Institute for Climate Change and Adaptation, University of Nairobi, Nairobi, Kenya; **Ogutu, Gàlgalo, Dokata, and Kirui**—Kenya Meteorological Department, Nairobi, Kenya

T he East African climate system has puzzled meteorologists and climate scientists for decades (Trewartha 1961). While East Africa straddles the equator at the same latitude as the planet's convective hotspots (including the Amazon and Congo Rainforest), it is predominantly semiarid or arid. The Chalbi Desert, in the Turkana Channel of northwest Kenya exemplifies this peculiarity, as the world's lowest-latitude desert (Fig. 1). A central player in the aridity is a large-scale (10^3 km) feature of the African climate system: the Turkana low-level jet (LLJ) (Fig. 2). The jet is responsible for approximately a third of water vapor transported from the Indian Ocean across the East African Rift System to the continental interior (Viste and Sorteberg 2013; Munday et al. 2021). It is also associated with widespread low-level divergence across East Africa, and the relatively low equatorial rainfall totals in Kenya (Nicholson 2016).

The only direct observations of the Turkana LLJ come from daytime pilot balloon (PiBAL) measurements made in the 1980s by the Kenya Meteorological Department (Kinuthia and Asnani 1982; Kinuthia 1992). These pioneering observations confirm the presence of the jet, but do not reveal the full diurnal cycle, quantify the jet-related water vapor fluxes, or document the thermodynamic environment associated with jet formation. One consequence of the paucity of observations is worrying disagreement among the latest reanalysis and model datasets in their estimates of jet speed (Nicholson 2016; Vizy and Cook 2019; King et al. 2021). Wind speeds from the PiBAL data in the 1980s are consistently higher—by 25% to 75%—compared to reanalysis estimates (Nicholson 2016). The observational void is particularly stark when compared with a jet of similar length scale in the United States—the Great Plains LLJ—which has been the subject of numerous field campaigns, and has a 40-yr climatology based on 36 rawinsonde stations (Walters et al. 2008). Of the three upper-air stations reporting to the global telecommunications system (GTS) in East Africa (in Nairobi, Addis Ababa, Dar es Salaam), none captures the Turkana jet (Fig. 2).
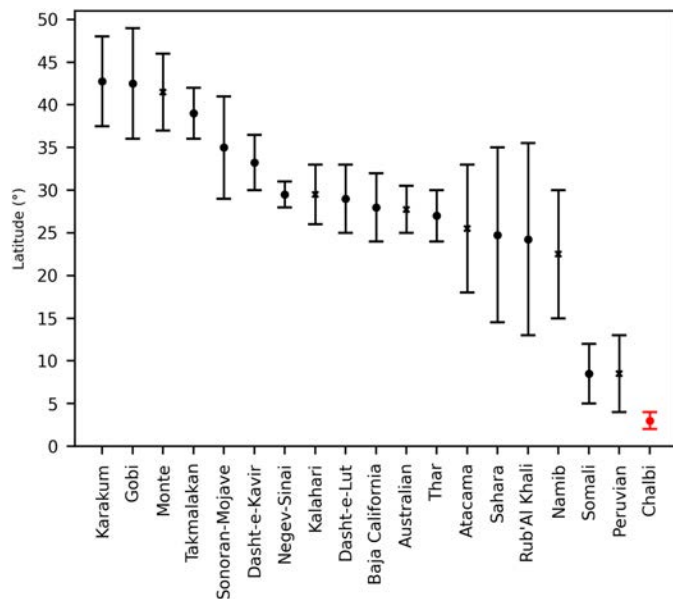
Fig. 1. **Latitudinal extent of deserts between 50°S and 50°N. Deserts are defined where annual rainfall < 200 mm based on CHIRPS rainfall data from Funk et al. (2015). Bars indicate latitudinal extent, and markers show central latitude. Crosses denote deserts in the Southern Hemisphere, and dots denote deserts in the Northern Hemisphere.**
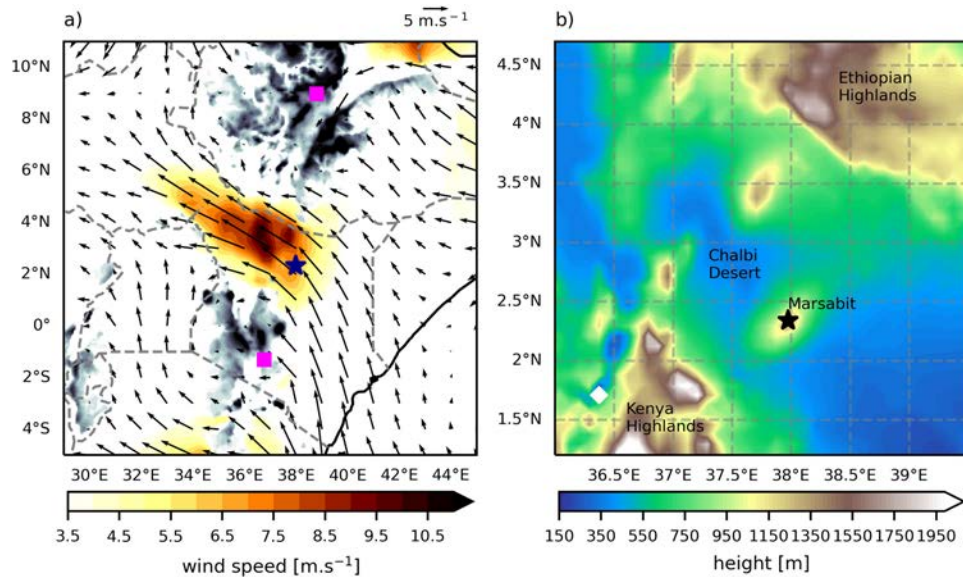
Fig. 2. (a) 850 hPa wind vectors and wind speed above 3.5 m s⁻¹ (orange shading), during 26 Mar–23 Apr 2021, showing the location of the Turkana jet. Surface heights above 1,500 m are in gray shading, the blue star is the location of field site (Marsabit), and the pink squares are the locations of existing radiosonde stations: Addis Ababa, Ethiopia (north), and Nairobi, Kenya (south). (b) Turkana Channel surface heights (m) from NASA GTOPO30 (http://earthexplorer.usgs.gov/).

One way to circumvent structural problems in observational coverage is through intensive observational periods targeted at important regions or features of the circulation. In Africa, such campaigns for data sparse regions, including the BoDEx project (Washington et al. 2006), the Fennec campaign in the Sahara (Washington et al. 2013; Marsham et al. 2013), and Africa Monsoon Multidisciplinary Analysis (AMMA) in West Africa (Redelsperger et al. 2006), have yielded fundamental new insights into the operation of regional climate. These campaigns also demonstrate the central role played by low-level jets in numerous Earth system processes, including water vapor transport (Lothon et al. 2008) and dust emission (Allen and Washington 2014; Washington et al. 2006).

In this paper, we give preliminary results for an intensive observational period (IOP) in NW Kenya to measure the Turkana LLJ—The Radiosonde Investigation for the Turkana Jet (RIFTJet). RIFTJet ran from 26 March to 23 April 2021, and has three core aims:

1) To observe the full diurnal cycle of the Turkana jet
2) To quantify moisture transport associated with the jet
3) To capture the thermodynamic/dynamic environment associated with jet formation and diurnal variability

Background: The Turkana jet

J. H. Kinuthia, who first identified the Turkana jet, was a Kenya Meteorological Department officer based in Nairobi responsible for quality control of the pilot balloon data from WMO stations across Kenya. After puzzling over the data from Marsabit, northwest Kenya, because of the unusually high wind speeds, he made the 1,200 km round trip from Nairobi to see for himself (R. A. Gàlgalo 2021, personal communication). While there, he confirmed the strong winds and wrote the first paper on the Turkana jet in 1982 (Kinuthia and Asnani 1982). Marsabit (2.3°N, 37.9°E; 1,337 m) is at the jet entrance region (Fig. 2), with the 1980s PiBAL data suggesting average annual jet strength of 17.5 m s⁻¹ at 0900 LT (Kinuthia and Asnani 1982). The observed pilot balloon data at Marsabit—which generally only reached ~3,000 m above ground level (AGL)—reveal occasions when there is a double jet core in the

vertical: one southeasterly jet below 800 hPa (the Turkana jet) and another northeasterly jet at 650 hPa (Kinuthia 1992).

Since the discovery of the Turkana jet, a handful of studies have considered the mechanisms leading to its formation. In a follow-up observational PiBAL study at different locations along the Turkana Channel (February 1983, June–July 1984), Kinuthia (1992) finds that the jet strengthens in regions where the channel—between the Kenya and Ethiopian Highlands—narrows. This implies that the jet is forced to the first order by orographic channeling (i.e., the Bernoulli theorem). Subsequent model experiments during the short rains (October–December) (Indeje et al. 2001) showed that orographic forcing is crucial for jet strength, while the depth and width of the channel help determine its location and vertical structure.

The model experiments also demonstrated that thermal and frictional forcing is crucial for jet maintenance (Indeje et al. 2001). Hartman (2018) argues, based on reanalysis data, that the along channel thermal gradient is critical for determining the annual cycle of jet strength, while Vizy and Cook (2019) show that a steeper thermal gradient is associated with a stronger jet on intraseasonal time scales. A steep horizontal pressure gradient, induced by thermal differences between jet entrance and jet exit regions, is important for the formation and strength of other equatorial nocturnal low-level jets, including in the Amazon (Greco et al. 1992).

Other possible mechanisms for jet maintenance and variability are difficult to test using reanalysis and model data. For example, inversions are crucial for jet development in many regions across the world (e.g., Blackadar 1957; Andreas et al. 2000), including near the equator (Greco et al. 1992), but are poorly resolved in reanalysis and model datasets with relatively coarse vertical resolution. Radiosonde data offer the possibility of observing inversions and their relation with jet activity.

The role of the Turkana LLJ in regional climate has received some attention. Kinuthia (1992) first suggested that the jet-related divergence could be responsible for the low rainfall totals in the Turkana Channel. Indeje et al.'s (2001) model experiments confirmed a link between divergence and subsidence in the channel, while Nicholson (2016) shows in reanalysis/satellite data that divergence in the Turkana Channel likely inhibits the development of a summer (June–August) rainfall season. At interannual time scales, Munday et al. (2021) and King et al. (2021) demonstrate that years when the jet is strong tend to be dry over East Africa, apart from in October (King et al. 2021). Meanwhile, Vizy and Cook (2019) link intraseasonal variability of the jet to rainfall in August, showing that rainfall is lower at the jet exit region over South Sudan when the jet is strong. A weakening of the Turkana jet over the last 40 years is present in some reanalysis products (MERRA-2 and JRA-55) (King et al. 2021) and could have implications for regional rainfall trends.

The Turkana LLJ plays an important role in African hydroclimate at larger scales too. Based on reanalysis data, Viste and Sorteberg (2013) and Munday et al. (2021) show that the Turkana LLJ is a key conduit for water vapor transport to the African interior. Viste and Sorteberg (2013) suggest that close to a third of water vapor for July–August rainfall over the Ethiopian Highlands (a hotspot of African convection; Hart et al. 2019) travels through the Turkana Channel. During April, Munday et al. (2021) show, based on MERRA-2 data, that the jet is responsible for ~63% of the low-level (below 700 hPa) water vapor export from an upstream region over Kenya. Observations of the Turkana LLJ could therefore inform our understanding of climate processes operating at a range of scales, several beyond the location of the jet itself.

The RIFTJet intensive observation period

Observations. A team of 12 took part in the IOP at the Marsabit WMO station (63641), the location of the 1980s pilot balloon releases (Fig. 2). The Marsabit WMO station is located on the northeastern slope of Mount Marsabit, a balsaltic shield volcano, at an elevation of 1,337 m.

After a pilot trip in January 2020, before the onset of the coronavirus pandemic, the field campaign was delayed to 2021, with observations commencing on 26 March and ending on 23 April 2021. We chose April because it is the time of year with the greatest intraseasonal variability in the jet strength, and because it is the normal time of rainfall onset over the region. The majority of observations comes from GRAW radiosondes (DFM-17 and DFM-09), which provide both winds and the thermodynamic structure of the atmosphere (temperature and humidity).
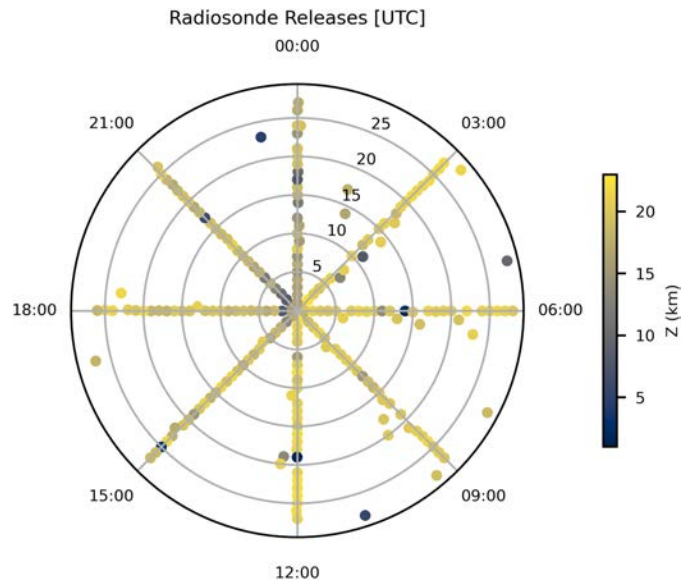
Starting at 2100 LT 26 March 2021, we released a radiosonde every 3 h until 1200 LT 23 April 2021. This approach allowed us to sample the diurnal cycle of winds and the atmospheric profile in unprecedented detail. Figure 3 summarizes the release times and indicates the balloon burst height: the sondes reached a median height of 19.8 km, mainly above the tropopause. In addition to the core releases at Marsabit, we conducted two releases at a location 60 km to the northeast, close to the village of Bubisa (literally "place of strong winds"). Bubisa (2.65°N, 38.0°E; 620 m MSL) is at a lower altitude than Marsabit and is in the center of the Turkana Channel, on the eastern edge of the Chalbi Desert. Including the two Bubisa sondes and some higher frequency measurements on the final morning of the campaign, we released 234 radiosondes.

Fig. 3. Radiosonde releases during RIFTJet. Each dot represents one radiosonde release, with release time (UTC) around circumference and day of IOP on radius. Colors indicate the height of balloon burst (km). The figure includes higher-frequency releases on the last IOP morning and two releases at Bubisa at 0130 UTC.

We calculate the integrated water vapor transport (IVT; kg m^{-1} s^{-1}) in radiosonde data as

$$\mathrm{IVT} = \sqrt{\left[\left(\frac{1}{g}\int_{\text{surface}}^{100\,\text{hPa}} qu\,dp\right)^2 + \left(\frac{1}{g}\int_{\text{surface}}^{100\,\text{hPa}} qv\,dp\right)^2\right]}, \quad (1)$$

where u and v are the zonal and meridional winds, q is the specific humidity, dp is the pressure increment, and g is the gravitational acceleration. In radiosonde data, we take the surface value as the first recorded measurement, and we integrate to 100 hPa. We give the relationship between pressure and height for standard pressure levels in Table 1.

Minute-resolution surface data from Marsabit at 2 and 10 m heights for wind speed, wind direction, pressure, temperature, humidity, rainfall, and solar radiation (2 m only) supplemented the regular radiosonde release schedule. Two Davis weather

Table 1. Average height (m) at selected pressure levels, derived from radiosonde data. Note that the surface at Marsabit is 1337 m (~866 hPa).

Pressure level (hPa)	Height (m)
850	1,486
800	2,010
700	3,144
600	4,409
500	5,861
400	7,581
300	9,694
200	12,444
150	14,283
100	16,588
70	18,613

The RIFTJet collaboration

RIFTJet comprised a small team of 12 staff and students from University of Oxford, University of Nairobi, and the Kenya Meteorological Department. With radiosondes releases every 3 h, there was some downtime in between releases to embark of an informal program of training.

In addition to the AWSs and radiosondes, we happened across the old theodolite used by Kinuthia and others for pilot balloon tracking in the 1980s (Fig. SB1) at the Marsabit weather station. One of us, with experience of using theodolites to measure another low-level jet in the Sahara, trained up the team and we ended up completing a number of pilot balloon tracks concurrently with the radiosonde releases. A project in the pipeline is to compare the pilot balloon tracks with the radiosonde data, and to reevaluate the old tracks from the 1980s.

Fig. SB1. (top) Pilot balloon tracking using Kinuthia's theodolite. (bottom) The RIFTJet team gathers for one of the final balloon releases.

Alongside equipment use, we also undertook training in data analysis in Python, covering how to read and analyze radiosonde and reanalysis data. The University of Nairobi Masters students completed the coding training course online, alongside other students from University of Oxford, during May and June 2021.

stations provided the surface measurements. Alongside the measurements, we conducted a program of training activities (see the sidebar), with all team members involved.

Large-scale meteorological setting during RIFTJet. In March–April 2021, the rainfall onset was delayed across Kenya, with widespread rainfall deficits during the observational period (Fig. 4). According to Climate Hazard Infrared Precipitation with Stations (CHIRPS) data (Funk et al. 2015), in the March–May ("long" rains) season, rainfall was less than 70% of normal across much of eastern and northern Kenya and Somalia, with delayed onset by

between 20 and 30 days (https://fews.net/east-africa/seasonal-monitor/june-2021). During the IOP, the 2 m AWS in Marsabit recorded three major rainfall events measuring a total of 70 mm. The long-term rainfall record at Marsabit corroborates the rainfall deficits. In the 2021 "long" rains, negative anomalies at Marsabit, were −46.0 mm (March), −163.2 mm (April), and −48.1 mm (May), compared to the 1981–2010 climatology.

The low rainfall is consistent with the Madden–Julian oscillation (MJO) phases (5 to 8) during IOP, which generally correspond to a lower probability of rainfall over the Turkana Channel during March–May (MacLeod et al. 2021). Negative SST anomalies (−0.5 to 1 K) were present in the tropical
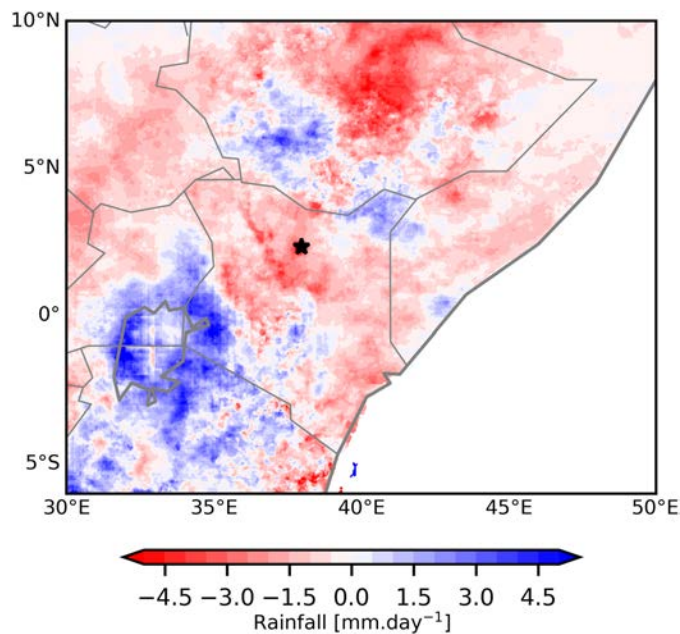

Fig. 4. Rainfall anomaly (mm day⁻¹) for 26 Mar–23 Apr 2021 compared to the climatology for the same period (1981–2010) from CHIRPS data. Black star indicates Marsabit location.

Atlantic during March 2021 (not shown), and commonly accompany later onset of rainfall in March–April (Nicholson 2017). In terms of the circulation, according to ERA5, the fastest average speed at 850 hPa (the approximate height of the jet core) through the channel during the IOP was ~10 m s⁻¹ (Fig. 2), which is within 0.5 m s⁻¹ of the ERA5 climatology (not shown).

Initial results and scientific outlook
Diurnal cycle of the Turkana jet. Maximum wind speed and vertical shear are common criteria used to detect LLJs (e.g., Whiteman et al. 1997; Rife et al. 2010; Allen and Washington 2014; Montini et al. 2019; Yan et al. 2021).

Here, we detect a low-level jet if the shear in the 800 m above a low-level wind maximum (≥ 8 m s⁻¹; $\leq 1,000$ m AGL) is at least 4 m s⁻¹. This conservative jet detection method allows us to identify low-level jets across a range of strengths, while preventing spurious detection of jets in the presence of fast wind speeds alone.

Seventy-two percent of soundings featured a low-level jet, with LLJs forming regularly throughout the diurnal cycle (Fig. 5) and on every night of the IOP. Jet frequency peaks during the night (0300 LT, 93%), but does not drop below 50% during the day. At 0300 LT, the average maximum wind speed is 16.8 m s⁻¹, and the average wind
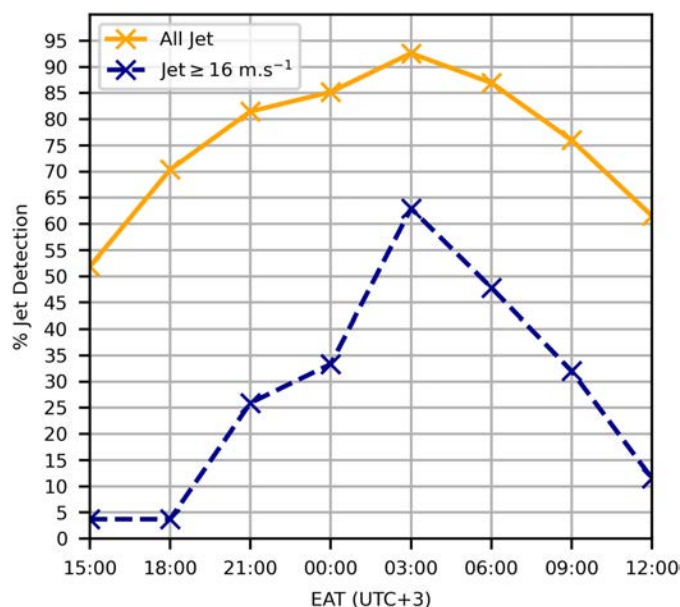

Fig. 5. Diurnal cycle of LLJ detection frequency (%). Orange line is for all detected LLJs; blue line is for strong jets ≥ 16 m s⁻¹.

maximum height is 300 m above the surface (~840 hPa). At 1500 LT, the average wind maximum rises to 600 m above the surface (~820 hPa), and the wind speed maximum reduces by 35% to 11.0 m s⁻¹. A consequence of the reduction in average wind speed during the day is a sharper diurnal cycle in the frequency of stronger LLJs (≥16 m s⁻¹). The strong jets were present on 63% of days at 0300 LT, while occurring once at 1500 and 1800 LT. The fastest recorded jet of 23.1 m s⁻¹ was observed at 0300 LT 11 April 2021.

A goal of the campaign is to evaluate reanalysis with respect to the observed data from Marsabit. Here, we focus our comparison on the latest-generation ECMWF reanalysis dataset—ERA5 (Hersbach et al. 2020)—which has the highest resolution (~30 km grid) of current global reanalysis. One factor influencing the comparison is the difference in surface pressure between ERA5 and reality (Fig. 6). While observations show that the Marsabit surface pressure is ~866 hPa, ERA5 data, bilinearly interpolated to the radiosonde release site, simulate
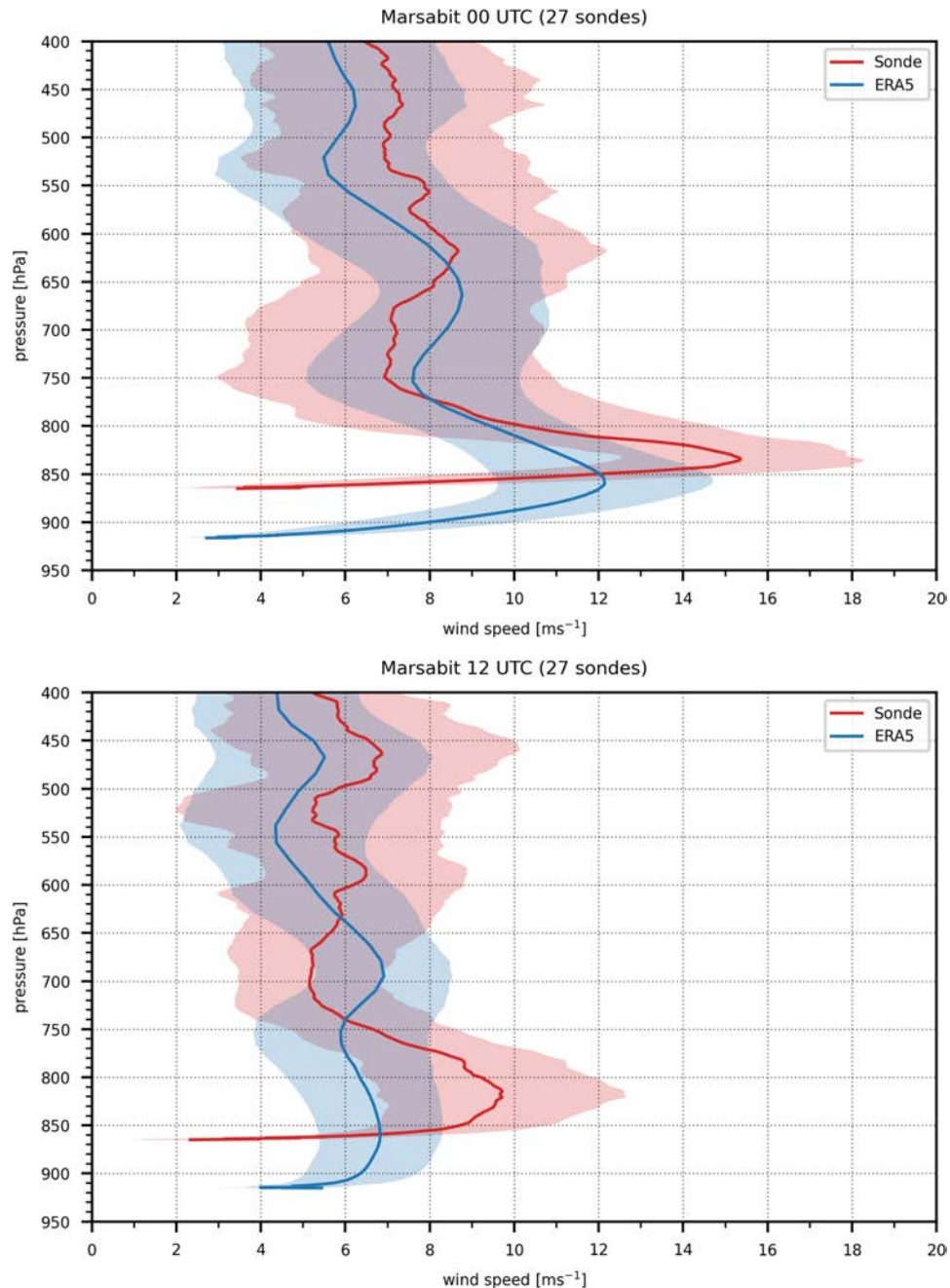
Fig. 6. Vertical wind speed profile in radiosondes (red) and ERA5 (blue) at Marsabit for (a) 0000 UTC (0300 LT) and (b) 1200 UTC (1500 LT). Shading indicates the standard deviation of winds at a given atmospheric level.

surface pressure at 925 hPa or lower. The lower surface elevation in ERA5 (799 m) compared to reality (1,337 m) is the most likely explanation for this discrepancy. The 538 m difference in surface height occurs in spite of the relatively high resolution of ERA5.

A key question is whether reanalysis data are able to reproduce the correct jet structure and speed. Figure 6 compares the average wind profile for radiosonde data and ERA5, at the hour of jet frequency minimum (1500 LT) and maximum (0300 LT). Across both comparisons, the height of the jet (above sea level) is lower in ERA5 compared to observations at Marsabit, due to the issues in representing surface pressure noted above. However, if we consider the height of the wind maximum above the surface (not shown), the ERA5 data simulate the jet maximum height at 0300 LT at 600 m above the ground, which is 300 m higher than the radiosonde-derived jet maximum height (300 m).

Apart from the structural differences, ERA5 simulates a low-level wind maximum that is one-third weaker than the observed maximum at 1500 LT (7.4 m s^{-1}) and ~24% weaker at 0300 LT (12.7 m s^{-1}). Indeed, at 1500 LT observations show a clear LLJ structure, which is not present in ERA5. This suggests that ERA5 does not capture the diurnal persistence of the jet, which is clear in observations (Fig. 5). At 0300 LT, ERA5 does simulate a low-level jet structure although the nose of the jet is somewhat broader in the vertical than observed, perhaps related to the limited vertical resolution of the reanalysis data (ERA5 model level data were used). While there are uncertainties in comparing gridded data to a point observation, the differences between ERA5 and radiosonde data here are significant and consistent across the grid boxes surrounding Marsabit (not shown). This emphasizes the need to treat reanalysis data critically in this part of the world.

Water vapor transport. LLJs are a key transport mechanism for water vapor in the lower atmosphere, and thus can be important for regional moisture budgets. The Great Plains low-level jet in the United States provides ~70%–80% of moisture to southern Great Plains region during jet events (Algarra et al. 2019), while the South American low-level jet is crucial in water vapor supply and downstream convective development (Vera et al. 2006; Sasaki et al. 2022). Reanalysis and model data indicate that the Turkana LLJ plays a central role in the East African moisture budget (Viste and Sorteberg 2013; Vizy and Cook 2019; Munday et al. 2021). Unlike the jets in North and South America, however, there has been no observational confirmation of the water vapor transport associated with the Turkana jet, nor has there been independent assessment of model and reanalysis data. Addressing these issues is a core aim of RIFTJet.

The role of the Turkana jet in water vapor transport is clear in the radiosonde data (Fig. 7). The maximum in water vapor transport through the column (>0.15 kg kg^{-1} m s^{-1}) is collocated with the height of the low-level jet, and there is a 36% increase in the maximum flux between 1500 and 0300 LT, corresponding with the jet strengthening during the night (Fig. 8). The consistently high moisture transport through the IOP provides observational confirmation that the Turkana jet is a key player in the regional moisture budget. While the maximum in water vapor transport relates to the low-level jet, there is significant transport, and diurnal variability, up to ~600 hPa. Water vapor transport at ~700 hPa peaks through the morning between 0600 and 1200 LT. The northeasterly flow at this level (see Fig. 9), and its diurnal variability, could explain the morning peak in water vapor flux.

A sounding in Bubisa, at the eastern edge of the Chalbi Desert, provides a clear example of the high IVT through the Turkana Channel (Fig. 9). The maximum in water vapor flux is collocated with the low-level (southeasterly) jet core, although significant moisture transport occurs up to 600 hPa. A distinct second maximum in moisture transport relates to a second (northeasterly) jet between 700 and 600 hPa. The northeasterly jet is the same as identified by Kinuthia (1992) in PiBAL releases at Marsabit. A third, easterly jet, with a maximum at
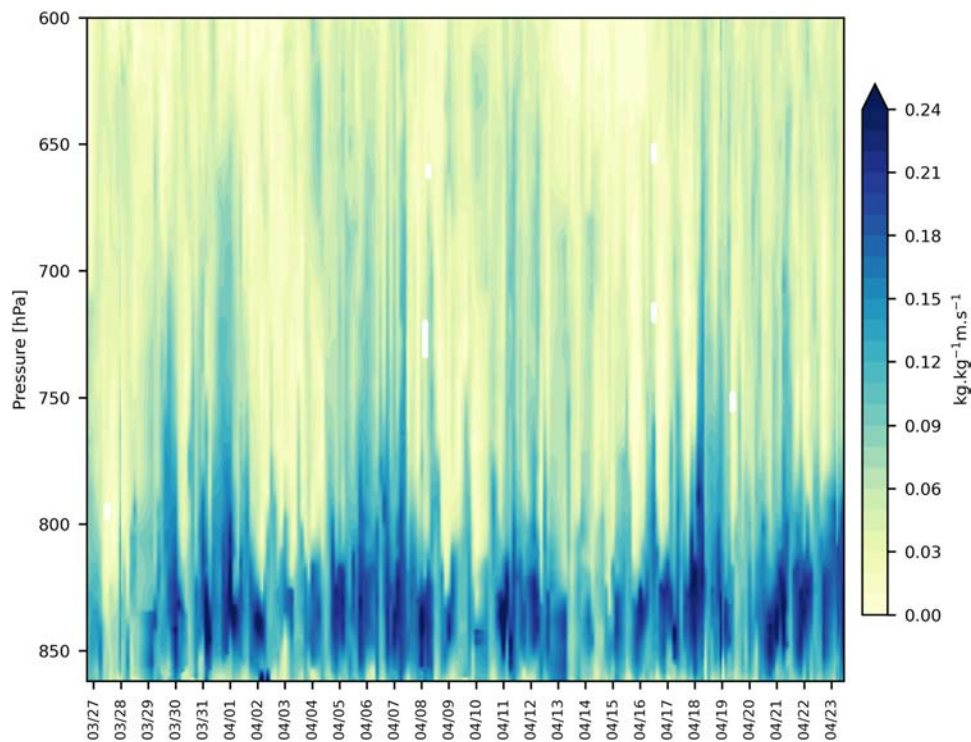
Fig. 7. Time–height Hovmöller diagram of water vapor flux (kg⁻¹ m s⁻¹) at 3-hourly intervals through the IOP, from radiosonde data.

7 km, is too high to be significant for water vapor flux. The column IVT of 328.0 kg m⁻¹ s⁻¹ is comparable in magnitude to weak atmospheric river events over oceans.

Reassuringly, ERA5 data from the same time do capture the significant water vapor flux through the channel, with the maximum in water vapor flux located ~250 km downstream of the sounding in Bubisa (Fig. 9). While ERA5 does capture high moisture flux at Bubisa, the IVT (283.4 kg m s⁻¹) is underestimated by 14% (44.6 kg m s⁻¹) compared to the radiosonde data. Such errors have the potential to cause biases in the regional moisture budget. A full assessment of water vapor transport in radiosondes and multiple reanalysis simulations across the whole IOP is the subject of a future paper.

Temperature inversions and thermodynamic environments. Understanding the mechanisms of jet formation is a main goal of RIFTJet. One focus is on the role of temperature inversions, which are closely related to jet formation and maintenance in other world regions (Blackadar 1957; Greco et al. 1992; Andreas et al. 2000; Baas et al. 2009; Van de Wiel et al. 2010). Figure 10 shows every recorded tropospheric temperature inversion for the RIFTJet period. Inversions occur
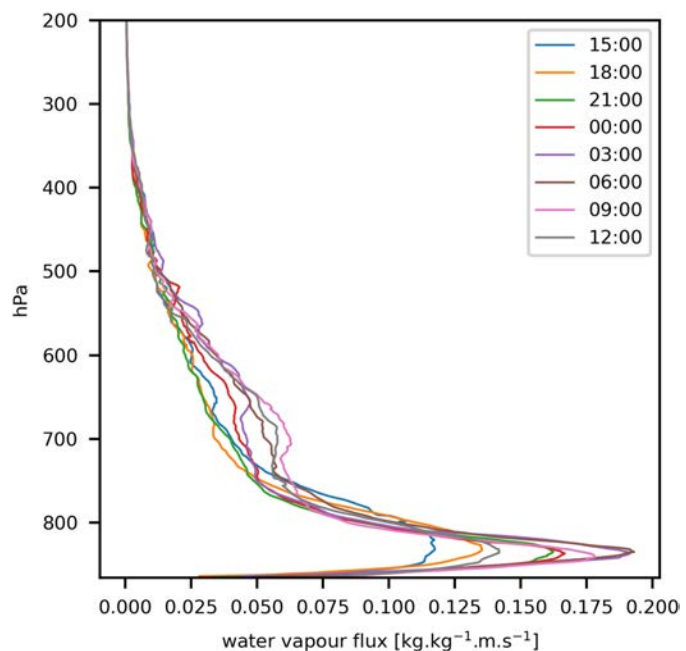

Fig. 8. Vertical profiles of water vapor flux (kg⁻¹ m s⁻¹) by time of day in radiosonde data.

at all heights, and can be split into three major types: surface-based inversions, near-surface inversions (at ~850 hPa), and upper-level inversions. Of these three types of inversion, the near-surface inversions are the strongest (~3°–8°C) and form at or very close to the height of the Turkana jet, preferentially during the night. The relationship between these inversions and jet dynamics are a focus of attention: reanalysis data, with relatively coarse vertical resolution, may struggle to capture the salient details.
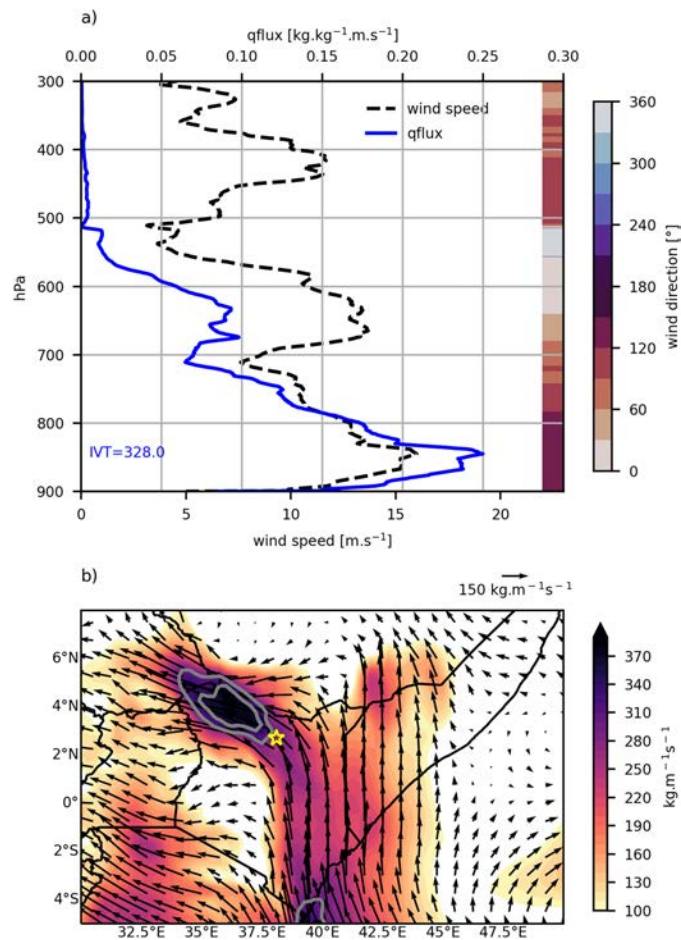
The surface based inversions tend to be weaker than the near-surface inversions, generally only reaching 1°C, with depths of less than 100 m. They form during the early evening with the onset of radiative cooling, and generally disappear by the early morning hours before sunrise. The diurnal cycle in surface-based inversions is clear in 2 and 10 m AWS data (Fig. 11). On average, the temperature inversion between 2 and 10 m starts developing before sunset around 1745 LT, reaching a maximum at midnight,

Fig. 9. (a) Radiosonde profile at Bubisa of winds (black dashed) and water vapor flux (blue solid) at 0445 LT 9 Apr 2021. Bar on the right side of the panel shows the vertical profile of wind direction (°). (b) ERA5 integrated water vapor transport (IVT; shading) at 0500 LT 9 Apr 2021. Contours show IVT at 300 and 350 kg m⁻¹. Yellow star indicates the location of the sounding.

before dissipating prior to sunrise at 0515 LT. The shear generated below the nocturnal jet, and associated turbulent mixing, is a possible cause of surface inversion breakdown prior to sunrise.

The upper-level inversions—concentrated between 600 and 400 hPa—are present throughout all days in the RIFTJet period. These are relatively weak (1°–3°C) and are likely dynamically induced by the large-scale tropospheric subsidence identified in reanalysis (Nicholson 2016) and model (Indeje et al. 2001) datasets. The subsidence places a key constraint on deep convection despite mean daytime CAPE in excess of 2,400 J kg⁻¹. Uncovering the origin of this subsidence, and its association with the Turkana jet and regional topography, is central to understanding the equatorial aridity in this region.

Conclusions

The RIFTJet campaign was a month-long field project, releasing 234 radiosondes in March and April 2021 to measure the diurnal cycle of the Turkana jet and the thermodynamic environment of the driest equatorial landmass on the planet. To the authors' knowledge, these are the first upper-air observations documenting the full diurnal cycle in the semi-arid region of East Africa.

The Turkana LLJ is a persistent feature of the atmospheric boundary layer in NW Kenya, present on 72% of the 3-hourly radiosondes. During the IOP, the peak jet speed occurred at 0300 LT, with an average maximum speed of 16.8 m s⁻¹. The jet continued to exist through
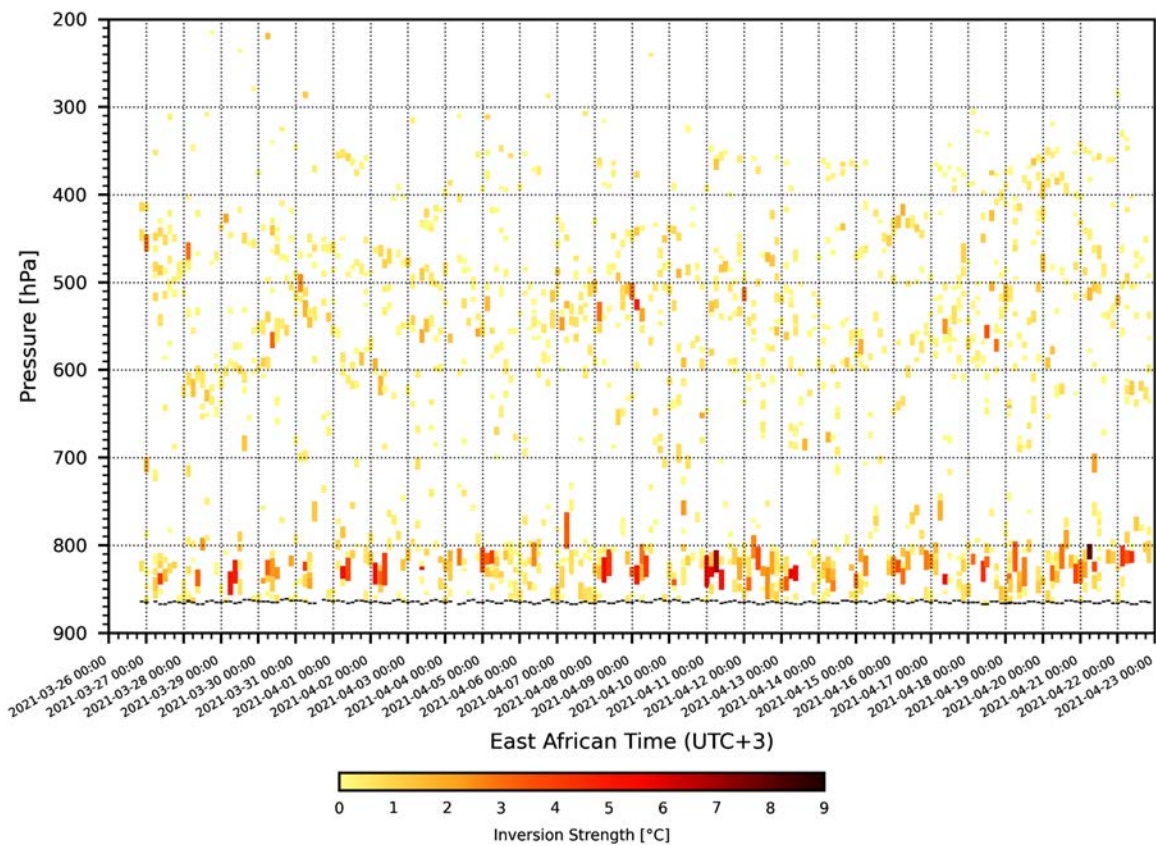
Fig. 10. Inversions by height across all 3-hourly radiosonde releases during the IOP. Inversion depth is given by the bars, and strength (°C) by the shading. The black dashed line shows the surface pressure (hPa).

the day 50% of the time. The radiosoundings confirmed significant jet-related water vapor transport, with pulses of elevated fluxes at low-levels in the night and in early morning.

The mean integrated water vapor flux measured at Marsabit across all radiosoundings is 172 kg m^{-1} s^{-1}. The fate of the water vapor and its role in downstream convection is not well known.

A principle purpose of the campaign is to evaluate and constrain model and reanalysis estimates of the Turkana LLJ. In this regard, preliminary analysis reveals that one of the latest-generation reanalysis products (ERA5) is able to capture the Turkana LLJ but underestimates its strength. The jet in ERA5 is 33% weaker than observed at 1500 LT. Ongoing analysis is assessing the reproduction of the full diurnal cycle in multiple reanalysis datasets to investigate whether this issue is systematic. This analysis will also consider whether the reanalysis
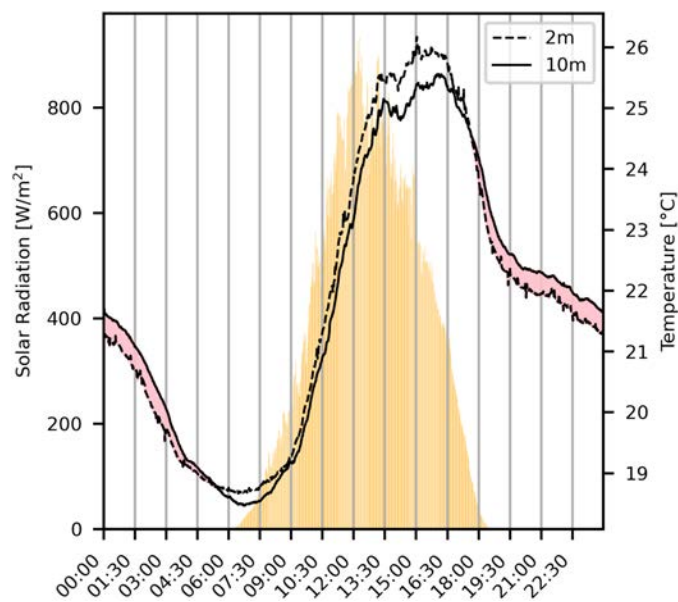

Fig. 11. Average diurnal cycle of temperature (°C) at 2 m (dashed) and 10 m (solid). Orange bars show solar radiation (W m^{-2}). Data are from automatic weather stations at 1-min resolution at local time (UTC + 3 h). Pink shading indicates times when there is a temperature inversion between 2 and 10 m.

data miss important processes that contribute to a strong jet in reality: one focus is the relationships between inversions and jet characteristics.

Constrained by logistical issues arising from a global pandemic, we were unable to conduct simultaneous observations at multiple sites or use a wider range of equipment. This constraint dictated the observational protocol such that we focused on high-temporal-resolution radiosonde releases from one location. In the end, this approach had a number of advantages, not least allowing us to sample the coevolution of the thermodynamic environment and winds throughout the diurnal cycle. In the future, direct measurements of vertical velocity, through LiDAR or sodar instrumentation, would complement the radiosonde data captured here.

The mission to understand the dynamics of the Turkana jet is at a nascent stage compared to other significant LLJs globally, including the South American LLJ and the Great Plains LLJ. The observations taken during RIFTJet provide a foundation for future observational and modeling work. Such work can help us build a more complete picture of the dynamics of the Turkana jet and its response to, and role in, a changing African climate system. Key questions remain unanswered and require further observation: What is the relationship between jet moisture transport and upstream/downstream convection? Do reanalysis data and climate models reproduce the correct annual cycle of the jet? What factors govern the variability of jet on seasonal and interannual time scales?

Finally, it is worth emphasizing that even after RIFTJet, we have better observations of LLJs in the Antarctic (population < 5,000; King 1989; Culf and McIlveen 1993; Andreas et al. 2000; Neff et al. 2008; Gallée et al. 2015; Vignon et al. 2019; Gorodetskaya et al. 2020) compared to those in East Africa (population 500 million). Alongside the Turkana LLJ in Kenya, there are at least four other major easterly low-level jets in eastern Africa from South Africa to Tanzania (Munday et al. 2021; Spavins-Hicks et al. 2021; Barimalala et al. 2021), none of which has been observed in any detail. These observations may prove crucial in providing reliable climate information in the face of rapid climate change over the next 20–50 years.

References

Algarra, I., J. Eiras-Barca, G. Miguez-Macho, R. Nieto, and L. Gimeno, 2019: On the assessment of the moisture transport by the Great Plains low-level jet. *Earth Syst. Dyn.*, **10**, 107–119, https://doi.org/10.5194/esd-10-107-2019.

Allen, C. J. T., and R. Washington, 2014: The low-level jet dust emission mechanism in the central Sahara: Observations from Bordj-Badji Mokhtar during the June 2011 Fennec intensive observation period. *J. Geophys. Res. Atmos.*, **119**, 2990–3015, https://doi.org/10.1002/2013JD020594.

Andreas, E. L., K. J. Claffey, and A. P. Makshtas, 2000: Low-level atmospheric jets and inversions over the western Weddell Sea. *Bound.-Layer Meteor.*, **97**, 459–486, https://doi.org/10.1023/A:1002793831076.

Baas, P., F. C. Bosveld, H. K. Baltink, and A. A. M. Holtslag, 2009: A climatology of nocturnal low-level jets at Cabauw. *J. Appl. Meteor. Climatol.*, **48**, 1627–1642, https://doi.org/10.1175/2009JAMC1965.1.

Barimalala, R., R. C. Blamey, F. Desbiolles, and C. J. C. Reason, 2021: The influence of southeastern African river valley jets on regional rainfall. *Climate Dyn.*, **57**, 2905–2920, https://doi.org/10.1007/s00382-021-05846-1.

Blackadar, A. K., 1957: Boundary layer wind maxima and their significance for the growth of nocturnal inversions. *Bull. Amer. Meteor. Soc.*, **38**, 283–290, https://doi.org/10.1175/1520-0477-38.5.283.

Culf, A., and J. F. McIlveen, 1993: Acoustic observation of the peripheral Antarctic boundary layer. *Waves and Turbulence in Stably Stratified Flows*, S. B. Mobbs and J. C. King, Eds., Clarendon Press, 139–154.

Funk, C., and Coauthors, 2015: The Climate Hazards Infrared Precipitation with Stations—A new environmental record for monitoring extremes. *Sci. Data*, **2**, 150066, https://doi.org/10.1038/sdata.2015.66.

Gallée, H., H. Barral, E. Vignon, and C. Genthon, 2015: A case study of a low-level jet during OPALE. *Atmos. Chem. Phys.*, **15**, 6237–6246, https://doi.org/10.5194/acp-15-6237-2015.

Gorodetskaya, I. V., T. Silva, H. Schmithüsen, and N. Hirasawa, 2020: Atmospheric river signatures in radiosonde profiles and reanalyses at the Dronning Maud Land Coast, East Antarctica. *Adv. Atmos. Sci.*, **37**, 455–476, https://doi.org/10.1007/s00376-020-9221-8.

Greco, S., S. Ulanski, M. Garstang, and S. Houston, 1992: Low-level nocturnal wind maximum over the central Amazon basin. *Bound.-Layer Meteor.*, **58**, 91–115, https://doi.org/10.1007/BF00120753.

Hart, N. C. G., R. Washington, and R. I. Maidment, 2019: Deep convection over Africa: Annual cycle, ENSO, and trends in the hotspots. *J. Climate*, **32**, 8791–8811, https://doi.org/10.1175/JCLI-D-19-0274.1.

Hartman, A. T., 2018: An analysis of the effects of temperatures and circulations on the strength of the low-level jet in the Turkana Channel in East Africa. *Theor. Appl. Climatol.*, **132**, 1003–1017, https://doi.org/10.1007/s00704-017-2121-x.

Hersbach, H., and Coauthors, 2020: The ERA5 global reanalysis. *Quart. J. Roy. Meteor. Soc.*, **146**, 1999–2049, https://doi.org/10.1002/qj.3803.

Indeje, M., F. H. M. Semazzi, L. Xie, and L. J. Ogallo, 2001: Mechanistic model simulations of the East African climate using NCAR regional climate model: Influence of large-scale orography on the Turkana low-level jet. *J. Climate*, **14**, 2710–2724, https://doi.org/10.1175/1520-0442(2001)014<2710:MMSOTE>2.0.CO;2.

King, J. A., S. Engelstaedter, R. Washington, and C. Munday, 2021: Variability of the Turkana low-level jet in reanalysis and models: Implications for rainfall. *J. Geophys. Res. Atmos.*, **126**, e2020JD034154, https://doi.org/10.1029/2020JD034154.

King, J. C., 1989: Low-level wind profiles at an Antarctic coastal station. *Antarct. Sci.*, **1**, 169–178, https://doi.org/10.1017/S095410208900026X.

Kinuthia, J. H., 1992: Horizontal and vertical structure of the Lake Turkana jet. *J. Appl. Meteor.*, **31**, 1248–1274, https://doi.org/10.1175/1520-0450(1992)031<1248:HAVSOT>2.0.CO;2.

——, and G. C. Asnani, 1982: A newly found jet in north Kenya (Turkana Channel). *Mon. Wea. Rev.*, **110**, 1722–1728, https://doi.org/10.1175/1520-0493(1982)110<1722:ANFJIN>2.0.CO;2.

Lothon, M., F. Saïd, F. Lohou, and B. Campistron, 2008: Observation of the diurnal cycle in the low troposphere of West Africa. *Mon. Wea. Rev.*, **136**, 3477–3500, https://doi.org/10.1175/2008MWR2427.1.

MacLeod, D. A., and Coauthors, 2021: Drivers and subseasonal predictability of heavy rainfall in equatorial East Africa and relationship with flood risk. *J. Hydrometeor.*, **22**, 887–903, https://doi.org/10.1175/JHM-D-20-0211.1.

Marsham, J. H., and Coauthors, 2013: Meteorology and dust in the central Sahara: Observations from Fennec supersite-1 during the June 2011 intensive observation period. *J. Geophys. Res. Atmos.*, **118**, 4069–4089, https://doi.org/10.1002/jgrd.50211.

Montini, T. L., C. Jones, and L. M. V. Carvalho, 2019: The South American low-level jet: A new climatology, variability, and changes. *J. Geophys. Res. Atmos.*, **124**, 1200–1218, https://doi.org/10.1029/2018JD029634.

Munday, C., R. Washington, and N. Hart, 2021: African low-level jets and their importance for water vapor transport and rainfall. *Geophys. Res. Lett.*, **48**, e2020GL090999, https://doi.org/10.1029/2020GL090999.

Neff, W., D. Helmig, A. Grachev, and D. Davis, 2008: A study of boundary layer behavior associated with high NO concentrations at the South Pole using a minisodar, tethered balloon, and sonic anemometer. *Atmos. Environ.*, **42**, 2762–2779, https://doi.org/10.1016/j.atmosenv.2007.01.033.

Nicholson, S., 2016: The Turkana low-level jet: Mean climatology and association with regional aridity. *Int. J. Climatol.*, **36**, 2598–2614, https://doi.org/10.1002/joc.4515.

——, 2017: Climate and climatic variability of rainfall over eastern Africa. *Rev. Geophys.*, **55**, 590–635, https://doi.org/10.1002/2016RG000544.

Redelsperger, J.-L., C. D. Thorncroft, A. Diedhiou, T. Lebel, D. J. Parker, and J. Polcher, 2006: African Monsoon Multidisciplinary Analysis: An international research project and field campaign. *Bull. Amer. Meteor. Soc.*, **87**, 1739–1746, https://doi.org/10.1175/BAMS-87-12-1739.

Rife, D. L., J. O. Pinto, A. J. Monaghan, C. Davis, and J. R. Hannan, 2010: Global distribution and characteristics of diurnally varying low-level jets. *J. Climate*, **23**, 5041–5064, https://doi.org/10.1175/2010JCLI3514.1.

Sasaki, C. R. S., A. K. Rowe, L. A. McMurdie, and K. L. Rasmussen, 2022: New insights into the South American low-level jet from RELAMPAGO observations. *Mon. Wea. Rev.*, **150**, 1247–1271, https://doi.org/10.1175/MWR-D-21-0161.1.

Spavins-Hicks, Z. D., R. Washington, and C. Munday, 2021: The Limpopo low-level jet: Mean climatology and role in water vapour transport. *J. Geophys. Res. Atmos.*, **126**, e2020JD034364, https://doi.org/10.1029/2020JD034364.

Trewartha, G. T., 1961: *The Earth's Problem Climates.* University of Wisconsin Press, 334 pp.

Van de Wiel, B. J. H., A. F. Moene, G. J. Steeneveld, P. Baas, F. C. Bosveld, and A. A. M. Holtslag, 2010: A conceptual view on inertial oscillations and nocturnal low-level jets. *J. Atmos. Sci.*, **67**, 2679–2689, https://doi.org/10.1175/2010JAS3289.1.

Vera, C., and Coauthors, 2006: The South American Low-Level Jet Experiment. *Bull. Amer. Meteor. Soc.*, **87**, 63–78, https://doi.org/10.1175/BAMS-87-1-63.

Vignon, É., O. Traullé, and A. Berne, 2019: On the fine vertical structure of the low troposphere over the coastal margins of East Antarctica. *Atmos. Chem. Phys.*, **19**, 4659–4683, https://doi.org/10.5194/acp-19-4659-2019.

Viste, E., and A. Sorteberg, 2013: Moisture transport into the Ethiopian highlands. *Int. J. Climatol.*, **33**, 249–263, https://doi.org/10.1002/joc.3409.

Vizy, E. K., and K. H. Cook, 2019: Observed relationship between the Turkana low-level jet and boreal summer convection. *Climate Dyn.*, **53**, 4037–4058, https://doi.org/10.1007/s00382-019-04769-2.

Walters, C. K., J. A. Winkler, R. P. Shadbolt, J. van Ravensway, and G. D. Bierly, 2008: A long-term climatology of southerly and northerly low-level jets for the central United States. *Ann. Assoc. Amer. Geogr.*, **98**, 521–552, https://doi.org/10.1080/00045600802046387.

Washington, R., M. C. Todd, S. Engelstaedter, S. Mbainayel, and F. Mitchell, 2006: Dust and the low-level circulation over the Bodélé Depression, Chad: Observations from BoDEx 2005. *J. Geophys. Res. Atmos.*, **111**, D03201, https://doi.org/10.1029/2005JD006502.

——, and Coauthors, 2013: Fennec—The Saharan Climate System: Project overview. *EGU General Assembly*, Vienna, Austria, European Geosciences Union, EGU2013-11570, https://meetingorganizer.copernicus.org/EGU2013/EGU2013-11570.pdf.

Whiteman, C. D., X. Bian, and S. Zhong, 1997: Low-level jet climatology from enhanced rawinsonde observations at a site in the Southern Great Plains. *J. Appl. Meteor.*, **36**, 1363–1376, https://doi.org/10.1175/1520-0450(1997)036<1363:LLJCFE>2.0.CO;2.

Yan, Y., X. Cai, X. Wang, Y. Miao, and Y. Song, 2021: Low-level jet climatology of China derived from long-term radiosonde observations. *J. Geophys. Res. Atmos.*, **126**, e2021JD035323, https://doi.org/10.1029/2021JD035323.